Reduced Basis Method for 2nd Order Wave Equation: Application to One-Dimensional Seismic Problem

Alex Y.K. Tan and A.T. Patera

***Abstract*— We solve the 2nd order wave equation, hyperbolic and linear in nature, for the pressure distribution of one-dimensional seismic problem with smooth initial pressure and rate of pressure change. The reduced basis method, offline-online computational procedures and *a posteriori* error estimation are developed. We show that the reduced basis pressure distribution is an accurate approximation to the finite element pressure distribution and the offline-online computational procedures work well. The *a posteriori* error estimation developed shows that the ratio of the maximum error bound over the maximum norm of the reduced basis error has a constant magnitude of $\mathcal{O}(10^2)$. The inverse problem works well, giving a "possibility region" of a set of system parameters where the actual system parameters may reside.**

***Index Terms*— hyperbolic equations, inverse problems, parameterized partial differential equations, reduced basis method.**

I. Introduction

ENGINEERING analysis requires prediction of outputs governed by partial differential equations. The reduced basis method is a promising answer to high computational cost which is inflexible in inverse problems. The reduced basis method was introduced in the 1970s for nonlinear structural analysis [1], [2], abstracted [3], [4], [5], [6] and extended [7], [8], [9] to a larger class of parameterized partial differential equations. Later works by Patera and co-workers [10], [11], [12], [13], [14] propose rigorous *a posteriori* error estimation and exploit the offline-online computational procedures. The reduced basis method has not been applied to hyperbolic problems because the nature of the solutions involve possibly discontinuous solution, weak stability properties and hence are more complicated. Simulations today play an important role in seismic research. Ghattas and co-workers [15], [16], [17], [18] aim to predict ground motion of large basins during strong earthquakes. In this paper, we examine a simplified one-dimensional seismic model, modified from [18].

II. Mathematical Model

A. Governing Equation

The pressure variation during an earthquake is governed by,

$$P^e_{o,tt}(x,t;\mu) - \kappa P^e_{o,xx}(x,t;\mu) = h(x;\mu)g(t;\mu), \qquad (1)$$

Alex Y.K. Tan is a student with Singapore-MIT Alliance, Computational Engineering Program.

A.T. Patera is Professor of Mechanical Engineering, Massachusetts Institute of Technology, MA 02139 USA; phone: 617 253 8122; fax: 617 258 5802; email: patera@mit.edu.

where $P^e_o(x,t;\mu)$ is the exact pressure distribution and κ is the wave propagation speed. The system parameters $\mu \equiv \{x_s, T\}$ are the earthquake source x_s and occurring time T and we vary them within the domain $\mathcal{D} \equiv [0.25, 0.75] \times [0.25, 0.75] \subset \mathbb{R}^2$.

In figure (1), the step function $h(x;\mu)$ and pulse function $g(t;\mu)$ characterize the spatial and temporal region of the earthquake source x_s with their integrals normalized to 1. The pulse function $g(t;\mu)$ are obtained based on its derivative, the hat function $g'(t;\mu)$. Time is normalized such that time $t = 4.1$ is a periodic cycle. The wave propagation speed κ is then normalized to 1 and the spatial domain is normalized to unit length, $\Omega_o(x_s) = [0,1]$.

The occurring time T shifts the pressure $P^e_o(x,t;\mu)$ in time and only play a role in the inverse problem. Thus, it is fixed as 0.50. The pressure is zero in the earth's crust $P^e_o(x = 0, t; x_s) = 0$ and the pressure gradient is zero on the earth's surface $P^e_{o,x}(x = 1, t; x_s) = 0$. Both initial pressure and rate of pressure change are zero, $P^e_o(x, t = 0; x_s) = P^e_{o,t}(x, t = 0; x_s) = 0$. Our focus is the dependence of the output,

$$\mathcal{S}^e_o(t; x_s) = \frac{1}{0.1}\int_{0.9}^{1.0} P^e_o(x,t;x_s)\, dx, \qquad (2)$$

the average surface pressure, on the earthquake source x_s.

B. Weak Form

The strong form is multiplied by a test function v and integrated in the spatial domain $\Omega_o(x_s)$. The integrals are further simplified using integration by parts, the divergence theorem and imposing the boundary conditions. The exact pressure distribution $P^e_o(x_s) \in \mathbf{X}^e_o(x_s) \equiv \{v \in \mathbf{H}^1(\Omega_o(x_s)) \mid v|_{\Gamma^D} = 0\}$ thus satisfies $\forall\ v \in \mathbf{X}^e_o(x_s)$,

$$m(P^e_{o,tt}(x_s), v; x_s) + a(P^e_o(x_s), v; x_s) \quad = \quad g(t)\tilde{h}(v), \qquad (3)$$

where $\forall\ w, v \in \mathbf{X}^e_o(x_s)$,

$$m(w, v; x_s) \quad \equiv \quad \int_{\Omega_o(x_s)} vw, \qquad (4)$$

$$a(w, v; x_s) \quad \equiv \quad \int_{\Omega_o(x_s)} v_x w_x, \qquad (5)$$

$$\tilde{h}(v) \quad \equiv \quad \int_{\Omega_o(x_s)} vh(x; x_s). \qquad (6)$$

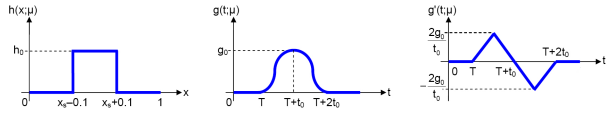

Fig. 1. Step function $h(x;\mu)$ (left), pulse function $g(t;\mu)$ (center) and hat function $g'(t;\mu)$ (right).

Our output is then evaluated as

$$\mathcal{S}_o^e(t;x_s) \quad = \quad \tilde{\ell}(P_o^e(x_s)), \tag{7}$$

where $\forall\ v \in \mathbf{X}_o^e(x_s)$,

$$\tilde{\ell}(v) = \frac{1}{0.1}\int_{0.9}^{1.0} v. \tag{8}$$

C. Reference Domain Formulation

We decompose the original x-domain $\Omega_o(x_s)$

$$\bar{\Omega}_o(x_s) = \bar{\Omega}_o^1(x_s) \cup \bar{\Omega}_o^2(x_s) \cup \bar{\Omega}_o^3(x_s) \cup \bar{\Omega}_o^4(x_s), \tag{9}$$

into the left zone $\Omega_o^1(x_s)$, forcing zone $\Omega_o^2(x_s)$, right zone $\Omega_o^3(x_s)$ and output zone $\Omega_o^4(x_s)$. We introduce the standard y-domain Ω in figure (2) as reference and decompose into

$$\bar{\Omega} = \bar{\Omega}^1 \cup \bar{\Omega}^2 \cup \bar{\Omega}^3 \cup \bar{\Omega}^4. \tag{10}$$

We now consider a piecewise affine mapping $\mathcal{F}$ from the standard y-domain Ω to the original x-domain $\Omega_o(x_s)$: $x = 2.5x_s y$ from Ω^1 to $\Omega_o^1(x_s)$; $x = y + x_s - 0.4$ from Ω^2 to $\Omega_o^2(x_s)$; $x = \frac{10}{3}(0.7-x_s)y+3x_s-1.2$ from Ω^3 to $\Omega_o^3(x_s)$; and the identity mapping from Ω^4 to $\Omega_o^4(x_s)$. Our exact pressure distribution $P_o^e(x,t;x_s)$ in the original x-domain $\Omega_o(x_s)$ can be expressed in the standard y-domain Ω as $P_o^e(x,t;x_s) = P^e(\mathcal{F}^{-1}(x),t;x_s)$.

Therefore, the exact pressure distribution $P^e(y,t;x_s) \in \mathbf{X}^e \equiv \{v \in \mathbf{H}^1(\Omega) \ \mid \ v|_{\Gamma^D} = 0\}$ in the standard y-domain Ω satisfies $\forall\ v \in \mathbf{X}^e$,

$$m(P_{tt}^e(x_s),v;x_s) + a(P^e(x_s),v;x_s) \quad = \quad g(t)\tilde{h}(v). \tag{11}$$

The output is then evaluated in terms of $P^e(y,t;x_s)$ as

$$\mathcal{S}^e(t;x_s) \quad = \quad \tilde{\ell}(P^e(x_s)). \tag{12}$$

D. Semi-Discretization for Time Marching

We use the unconditionally stable **Newmark** scheme and the weak form become $\forall\ v \in \mathbf{X}^e$,

$$m\left(\frac{P^{e,k}(x_s) - 2P^{e,k-1}(x_s) + P^{e,k-2}(x_s)}{\Delta t^2}, v; x_s\right) + a\left(\frac{P^{e,k}(x_s) + P^{e,k-2}(x_s)}{2}, v; x_s\right) = \frac{g^k + g^{k-2}}{2}\tilde{h}(v), \tag{13}$$

$$\mathcal{S}^{e,k}(x_s) \quad = \quad \tilde{\ell}(P^{e,k}(x_s)), \tag{14}$$

where the pressure distribution for the zero and first time steps are zero, $P^{e,0}(x_s) = P^{e,1}(x_s) = 0$.

III. Finite Element Method

A. Triangulation

We solve equation (13) using the Galerkin approach. With n triangles T_h, we define a "truth" $\mathbb{P}_1$ finite element approximation space $\mathbf{X}(\equiv \mathbf{X}_h) \subset \mathbf{X}^e : \{v \in \mathbf{X}^e \mid v|_{T_h} \in \mathbb{P}_1(T_h),\ \forall\ T_h \in \mathcal{T}_h\}$. This finite element space $\mathbf{X}$ (of dimension $\mathcal{N}$) is a sufficiently rich approximation subspace such that the different between the exact and finite element pressure distribution is small.

$P^k(x_s) \in \mathbf{X}$ is denoted as the fully discrete finite element approximation at time $t^k = k\Delta t$, where Δt is the time step size. Using the bilinear and linear properties of the various functions, the nodal coefficients $P_j^k(x_s)$ are solved from

$$\left\{\frac{1}{\Delta t^2}\mathbf{M}(x_s) + \frac{1}{2}\mathbf{A}(x_s)\right\}\mathbf{P}^k(x_s) = \left\{\frac{1}{\Delta t^2}\mathbf{M}(x_s)\left[2\mathbf{P}^{k-1}(x_s) - \mathbf{P}^{k-2}(x_s)\right] - \frac{1}{2}\mathbf{A}(x_s)\mathbf{P}^{k-2}(x_s) + \frac{g^k + g^{k-2}}{2}\mathbf{H}\right\}, \tag{15}$$

where $\mathbf{M}(x_s)$ is the mass matrix, $\mathbf{A}(x_s)$ is the stiffness matrix, $\mathbf{H}$ is the load vector and $\mathbf{L}$ is the output vector. The output is subsequently evaluated as

$$\mathcal{S}^k(x_s) \quad = \quad \mathbf{P}^k(x_s)^T\mathbf{L}. \tag{16}$$

B. Truth Approximation

The numerical parameters $\phi \equiv \{\mathcal{N}, \Delta t\}$ is taken to give the "truth" pressure distribution $P^{\mathcal{T},k}(x_s)$ and output $\mathcal{S}^{\mathcal{T},k}(x_s)$, upon which we develop our reduced basis method and *a posteriori* error estimation.

We now introduce the inner product $(\cdot,\cdot) \equiv (\cdot,\cdot)_{\mathbf{X}}$,

$$(w,v) \equiv a(w,v;x_s = 0.50), \tag{17}$$

and the associated norm $\|\cdot\| \equiv \|\cdot\|_{\mathbf{X}}$,

$$\|w\| \equiv \sqrt{(w,w)}. \tag{18}$$

$x_s = 0.50$ is used because it corresponds to identity mapping across the physical x-domain $\Omega_o(x_s)$ and standard y-domain Ω. From convergence analysis, the numerical parameters used are $\phi = \{\mathcal{N} = 200, \Delta t = 0.01\}$.

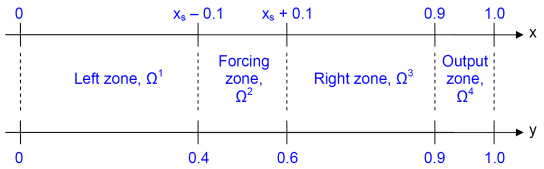

Fig. 2. Piecewise affine mapping $\mathcal{F}$ between the original x-domain $\Omega_o(x_s)$ and standard y-domain Ω.

IV. Reduced Basis Method

A. Formulation

We define the reduced basis space W_N (of dimension N) as the span of N finite element pressure distribution $\{P^{k_1}(x_{s_1}), \ldots, P^{k_N}(x_{s_N})\}$, selected within the training space $\Xi_{train} = \Xi^{x_s}_{train} \times \Xi^{k}_{train}$: an earthquake source-time space containing γ different values of the earthquake source x_s and all time steps. To prevent ill-conditioning, they are further orthogonalized using the modified Gram-Schmidt orthogonalization [19] to obtain

$$W_N \quad = \quad \text{span}\{\zeta_1, \ldots, \zeta_N\}. \tag{19}$$

The reduced basis pressure distribution $P^k_N(x_s) \in W_N \subset \mathbf{X}$ is given by simple Galerkin projection where the reduced basis pressure distribution $P^k_N(x_s)$ and test function v are now expressed in terms of the N orthogonalized finite element pressure distribution $\{\zeta_1, \ldots, \zeta_N\}$. Again using the bilinear and linear properties of the various functions, the reduced basis coefficients $\underline{P}^k_{N,j}(x_s)$ are solved from

$$\begin{aligned}\left\{\frac{1}{\Delta t^2}\mathbf{M}_N(x_s) + \frac{1}{2}\mathbf{A}_N(x_s)\right\}\underline{\mathbf{P}}^k_N(x_s) \\ = \left\{\frac{1}{\Delta t^2}\mathbf{M}_N(x_s)\left[2\underline{\mathbf{P}}^{k-1}_N(x_s) - \underline{\mathbf{P}}^{k-2}_N(x_s)\right]\right. \\ \left. - \frac{1}{2}\mathbf{A}_N(x_s)\underline{\mathbf{P}}^{k-2}_N(x_s) + \frac{g^k + g^{k-2}}{2}\mathbf{H}_N\right\},\end{aligned} \tag{20}$$

where $\mathbf{M}_N(x_s)$ is the reduced mass matrix, $\mathbf{A}_N(x_s)$ is the reduced stiffness matrix, $\mathbf{H}_N$ is the reduced load vector and $\mathbf{L}_N$ is the reduced output vector. The reduced basis output $\mathcal{S}^k_N(x_s)$ can then be evaluated as

$$\mathcal{S}^k_N(x_s) \quad = \quad \underline{\mathbf{P}}^k_N(x_s)^T\mathbf{L}_N. \tag{21}$$

B. Offline-Online Computational Procedures

The affine parametric structure of

$$\mathbf{M}_N(x_s)_{ij} = m(\zeta_j, \zeta_i; x_s) = \sum_{q=1}^{Q_m} \Theta^q_m(x_s) m^q(\zeta_j, \zeta_i), \tag{22}$$

$$\mathbf{A}_N(x_s)_{ij} = a(\zeta_j, \zeta_i; x_s) = \sum_{q=1}^{Q_a} \Theta^q_a(x_s) a^q(\zeta_j, \zeta_i), \tag{23}$$

can now be exploited to design effective offline-online computational procedures.

In the offline stage, the basis vectors $\{\zeta_1, \ldots, \zeta_N\}$ are first solved. Next, $m^q(\zeta_j, \zeta_i)$ and $a^q(\zeta_j, \zeta_i)$ are formed and stored for $1 \le i, j \le N, 1 \le q \le Q_m, Q_a$. In the online stage, for each new value of the earthquake source x_s, the reduced mass matrix $\mathbf{M}_N(x_s)$ and the reduced stiffness matrix $\mathbf{A}_N(x_s)$ are first assembled from equations (22) and (23). Next, reduced basis output $\mathcal{S}^k_N(x_s)$ is solved from equations (20) and (21). It is important to note that the offline stage is performed only once while the online stage is performed for different values of the earthquake source x_s. Since the online stage is independent of the dimension of the finite element space $\mathcal{N}$ which is large but rather dependent on the dimension of the reduced basis space N which is much smaller $N \ll \mathcal{N}$, significant reduction in computational cost is often expected.

C. Norms

The reduced basis error $e^k(x_s) = P^k(x_s) - P^k_N(x_s)$ is defined as the difference between the finite element $P^k(x_s)$ and reduced basis $P^k_N(x_s)$ pressure distribution with the corresponding norm as

$$\|e^k(x_s)\| = \|P^k(x_s) - P^k_N(x_s)\|. \tag{24}$$

The maximum norm of the reduced basis error in the training space Ξ_{train},

$$\|e\|_{tr,max} = \max_{x_s \in \Xi^{x_s}_{train}, k \in \Xi^k_{train}} \|e^k(x_s)\|, \tag{25}$$

is then the maximum value of the norm of the reduced basis error $\|e^k(x_s)\|$ throughout the training space Ξ_{train}.

Similarly, the maximum norm of the reduced basis error in the test space Ξ_{test},

$$\|e\|_{te,max} = \max_{x_s \in \Xi^{x_s}_{test}, k \in \Xi^k_{test}} \|e^k(x_s)\|, \tag{26}$$

is the maximum value of the norm of the reduced basis error $\|e^k(x_s)\|$ throughout the test space Ξ_{test}. The test space $\Xi_{test} = \Xi^{x_s}_{test} \times \Xi^k_{test}$ is an earthquake source-time space containing ρ different values of the earthquake source x_s and all time steps, where we perform the online stage.

Next, the projected pressure distribution $\Pi(P^k(x_s))$ is defined as the argument that minimizes the norm of the difference between vectors in the reduced basis space W_N and the finite element pressure distribution $P^k(x_s)$,

$$\Pi(P^k(x_s)) = \arg\min_{w \in W_N} \|w - P^k(x_s)\|. \tag{27}$$

The projection error $e^k_\Pi(x_s) = P^k(x_s) - \Pi(P^k(x_s))$ is then defined as the difference between the finite element $P^k(x_s)$ and projected $\Pi(P^k(x_s))$ pressure distribution with the corresponding norm as

$$\|e^k_\Pi(x_s)\| = \|P^k(x_s) - \Pi(P^k(x_s))\|. \tag{28}$$

Similarly, the maximum norm of the projection error

$$\|e_\Pi\|_{max} = \max_{x_s \in \Xi^{x_s}_{train}, k \in \Xi^k_{train}} \|e^k_\Pi(x_s)\|, \tag{29}$$

is the maximum value of the norm of the projection error $\|e^k_\Pi(x_s)\|$ throughout the training space Ξ_{train}.

D. Greedy Algorithm

The greedy algorithm selects basis vectors within the training space Ξ_{train} and the procedure is as followed:

Step 1. The first basis vector $P^{k_1}(x_{s_1})$ is fixed as the finite element pressure distribution $P^k(x_s)$ at the last time step $t = K\Delta t$, corresponding to the earthquake source $x_s = 0.50$.

Step 2. Modified Gram-Schmidt orthogonalization is performed.

Step 3. Equation (20) is solved in the training space Ξ_{train} to yield the reduced basis pressure distribution $\mathbf{P}^k_N(x_s)$.

Step 4. Determine the norm of the reduced basis error $\|e^k(x_s)\|$ and projection error $\|e^k_\Pi(x_s)\|$ from equations (24) and (28) respectively; obtain the maximum norm of the reduced basis error $\|e\|_{tr,max}$ and projection error $\|e_\Pi\|_{max}$.

Step 5. If the maximum norm of the reduced basis error $\|e\|_{tr,max}$ is less than the tolerance ε specified, the greedy algorithm terminates. Else, the finite element pressure distribution $P^k(x_s)$ that corresponds to the maximum norm of the projection error $\|e_\Pi\|_{max}$ will be the next basis vector and steps 2 to 4 are repeated.

In step 5, the maximum norm of the reduced basis error $\|e\|_{tr,max}$ is used as the terminating criteria because it gives the maximum error norm if the finite element method is used instead. Similarly, if the maximum norm of the reduced basis error $\|e\|_{tr,max}$ is used to select the next basis vector, the greedy algorithm will break down. This is because during time marching, a high value of the maximum norm of the reduced basis error $\|e\|_{tr,max}$ may be cause by an inaccurate reduced basis pressure distribution $P^k_N(x_s)$ at a previous time step. Hence, unless that previous time step is chosen as a basis vector, the maximum norm of the reduced basis error $\|e\|_{tr,max}$ will not drop. Selecting the next basis vector based on the maximum norm of the projection error $\|e_\Pi\|_{max}$ instead overcome this problem as the projection error $e^k_\Pi(x_s)$ does not have this time marching effect. However, this will lead to an increase in computational cost.

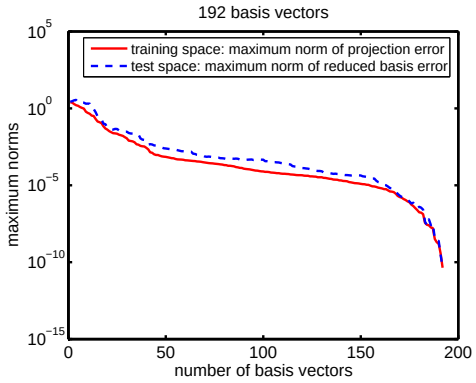

Fig. 3. Convergence rate of maximum norm of the projection error $\|e_\Pi\|_{max}$ in training space Ξ_{train} as well as maximum norm of the reduced basis error $\|e\|_{te,max}$ in test spaces Ξ_{test}.

E. Convergence Rate

14 different values of the earthquake source x_s, selected in equal logarithmic interval, are used to determine the performance of the greedy algorithm. From figure (3), the convergence rate can be separated into 3 stages. In stage 1, there is a period of rapid convergence where the maximum norm of the projection error $\|e_\Pi\|_{max}$ drops 3 orders of magnitude after 50 basis vectors are selected. This is followed by stage 2, a period of slow convergence where an addition of about 100 basis vectors are needed to have the same decrease in magnitude. Finally, stage 3 again has a fast convergence rate where an addition of roughly 30 basis vectors result in a drop of 4 orders of magnitude.

It is observed that the first 50 basis vectors are "general" such that other finite element pressure distribution $P^k(x_s)$ can be accurately expressed as a combination of them. Hence, the norm of the projection error $\|e^k_\Pi(x_s)\|$ drops rapidly and uniformly across the training space Ξ_{train} as in figure (4).

After these "general" basis vectors are added, the norm of the projection error $\|e^k_\Pi(x_s)\|$ becomes a U-shaped trough extending along the time-domain, with high "peaks" in the 2 extreme ends of the earthquake source space and a flat "basin" around the middle as in figure (5). The basis vectors selected are now mostly "specialize" and have little effect on the rest of the norm of the projection error $\|e^k_\Pi(x_s)\|$ in the training space Ξ_{train}. The greedy algorithm selects basis vectors alternately from these 2 extreme regions, eliminating the various "peaks" one by one, resulting in the slow convergence rate. After eliminating most of the "peaks", the norm of the projection error $\|e^k_\Pi(x_s)\|$ across the training space Ξ_{train} is now mostly uniform. Together with the additional basis vectors selected, the norm of the projection error $\|e^k_\Pi(x_s)\|$ drops rapidly.

Furthermore, it is observed that increasing the size of the training space γ or the dimension of the finite element space $\mathcal{N}$ or decreasing the time step size Δt result in an increase in the dimension of the reduced basis space N, which eventually tapped to roughly a constant value [19]. Lastly, increaseing

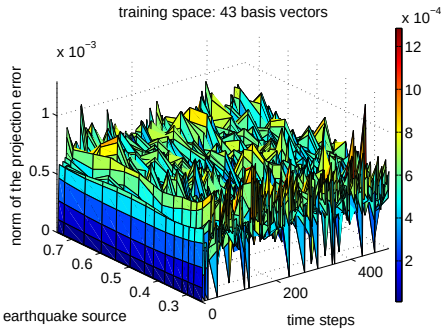

Fig. 4. Norm of the projection error $\|e^k_\Pi(x_s)\|$ in training space Ξ_{train} after selecting the 43rd basis vectors.

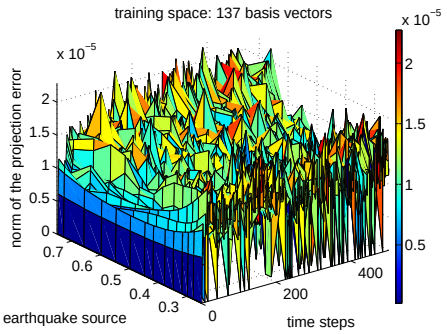

Fig. 5. Norm of the projection error $\|e^k_\Pi(x_s)\|$ in training space Ξ_{train} after selecting the 137th basis vectors.

the size of the test space ρ results in the same convergence rate.

F. Computational Cost

Due to the complexity of the offline stage, the operation counts are evaluated accordingly to the selection of the last basis vector ζ_N. Assuming that the operation counts for the finite element pressure distribution $P^k(x_s)$ scales as $C\mathcal{N}^\sigma$ for some σ presumably close to unity, we require $\mathcal{O}(\gamma CK\mathcal{N}^\sigma)$ operations. Obtaining the reduced basis pressure distribution $P^k_N(x_s)$ requires another $\mathcal{O}(\gamma KN\mathcal{N})$ operations. Hence, the offline stage for the selection of the last basis vector ζ_N will require $\mathcal{O}(\gamma CK\mathcal{N}^\sigma + \gamma KN\mathcal{N})$ operations.

After the completion of the offline stage, the decomposed reduced matrices and vectors are stored, with a storage counts of $\mathcal{O}((Q_m + Q_a)N^2)$. For the online stage, the left-hand-side matrix of equation (20) is first decomposed into an upper and lower triangular matrices using LU decomposition. Hence, for every time step, equation (20) is solved using forward and backward substitution, giving an operation counts of $\mathcal{O}(KN^2)$.

The time taken for the finite element method and the online stage is compared. Their operation counts are $\mathcal{O}(CK\mathcal{N}^\sigma)$ and $\mathcal{O}(KN^2)$ respectively. For the one-dimensional seismic problem, the dimension of the finite element space $\mathcal{N}$ used is 200 while the dimension of the reduced basis space N is 175 for a tolerance ε of 10^{-6}. Hence, the online stage will take a longer time compared to the finite element method. The efficiency of the offline-online computational procedure should be more evident when applied to the two-dimensional seismic problem where the dimension of the finite element space $\mathcal{N}$ is the square of its present value and the dimension of the reduced basis space N is expected to increase but still has the same order of magnitude.

V. *A Posteriori* Error Estimation

A. Formulation

We now develop rigorous and sharp *a posteriori* bounds to ensure a rigorously certified accuracy of the results. The *a posteriori* error estimation produces an error bound $\Delta^k_N(x_s)$ and output error bound $\Delta^k_{\mathcal{S},N}(x_s)$,

$$\|e^k(x_s)\| \equiv \|P^k(x_s) - P^k_N(x_s)\| \le \Delta^k_N(x_s), \tag{30}$$

$$e^k_{\mathcal{S}}(x_s) \equiv |\mathcal{S}^k(x_s) - \mathcal{S}^k_N(x_s)| \le \Delta^k_{\mathcal{S},N}(x_s), \tag{31}$$

where the reduced basis output error $e^k_{\mathcal{S}}(x_s)$ is the absolute difference between the finite element $\mathcal{S}^k(x_s)$ and reduced basis $\mathcal{S}^k_N(x_s)$ output. The maximum reduced basis output error

$$e_{\mathcal{S},max} = \max_{x_s\in\Xi^{x_s}_{test}, k\in\Xi^k_{test}} e^k_{\mathcal{S}}(x_s), \tag{32}$$

is the maximum value of the reduced basis output error $e^k_{\mathcal{S}}(x_s)$ throughout the test space Ξ_{test}.

From the reduced basis approximation, we derived the residual $r^k(v;x_s)$ and simplified it to the error-residual equation using the definition of the reduced basis error $e^k(x_s)$,

Error-Residual: $e^k(x_s) = P^k(x_s) - P^k_N(x_s), k = 2,\cdots,K$, $e^0(x_s) = e^1(x_s) = 0$,

$$m\left(\frac{e^k(x_s) - 2e^{k-1}(x_s) + 2e^{k-2}(x_s)}{\Delta t^2}, v; x_s\right) + a\left(\frac{e^k(x_s) + e^{k-2}(x_s)}{2}, v; x_s\right) = r^k(v;x_s). \tag{33}$$

Next, we simplified the summation of the mass, stiffness and residual functions from the 2nd to K time steps,

Lemma 1.1: for any $z^j, \quad j = 0,\cdots,n, \quad z^0 = z^1 = 0$,

$$\sum_{j=2}^{n} m\left(\frac{z^j - 2z^{j-1} + z^{j-2}}{\Delta t^2}, \frac{z^j - z^{j-2}}{2}; x_s\right) = \frac{1}{2} m\left(\frac{z^n - z^{n-1}}{\Delta t}, \frac{z^n - z^{n-1}}{\Delta t}; x_s\right), \tag{34}$$

Lemma 1.2: for any $z^j, \quad j = 0,\cdots,n, \quad z^0 = z^1 = 0$,

$$\sum_{j=2}^{n} a\left(\frac{z^j+z^{j-2}}{2}, \frac{z^j-z^{j-2}}{2}; x_s\right) = \frac{1}{4}\left[a(z^n, z^n; x_s) + a(z^{n-1}, z^{n-1}; x_s)\right], \quad (35)$$

Lemma 1.3: for any z^j satisfying the residual equation, $j = 0, \cdots, n, \quad z^0 = z^1 = 0,$

$$\sum_{j=2}^{n} r^j\left(\frac{z^j-z^{j-2}}{2}; x_s\right) = \frac{1}{2}\left[r^n(z^n; x_s) + r^{n-1}(z^{n-1}; x_s)\right] - \sum_{j=2}^{n}\frac{1}{2}(r^j - r^{j-2})(z^{j-2}; x_s). \quad (36)$$

Proof: From the left-hand-side of the 3 lemmas, use the bilinear and linear properties of the functions to separate the single function into several simpler functions. Cancelling of the same terms across different time step proved the lemmas.

Now we show that the stiffness function is coercive

$$a(w, w; x_s) \geq \alpha(x_s)\|w\|^2, \quad (37)$$

$$\alpha(x_s) \equiv \inf_{w\in\mathbf{X}} \frac{a(w, w; x_s)}{\|w\|^2} = \min_q \Theta_a^q(x_s), \quad (38)$$

and the coercivity constant $\alpha(x_s)$ takes the minimum of the system parameters-dependent function of the stiffness function $\Theta_a^q(x_s)$, $1 \leq q \leq Q_a$. The dual norm $\|\cdot\|_{\mathbf{X}'}$ is defined as

$$\|g\|_{\mathbf{X}'} \equiv \sup_{v\in\mathbf{X}} \frac{g(v)}{\|v\|}, \quad (39)$$

for any function v in the "truth" finite element space $\mathbf{X}$.

Lemma 2: $n = 2, \cdots, K, \quad \|e^0(x_s)\| = \|e^1(x_s)\| = 0,$

$$\|e^n(x_s)\|^2 \leq \left\{\frac{4}{\alpha(x_s)^2}\left(\|r^n(x_s)\|^2_{\mathbf{X}'} + \|r^{n-1}(x_s)\|^2_{\mathbf{X}'}\right) + \frac{8}{\alpha(x_s)}\Delta t\sum_{j=2}^{n}\left(\left\|\frac{(r^j - r^{j-2})(x_s)}{2\Delta t}\right\|_{\mathbf{X}'}\|e^{j-2}(x_s)\|\right)\right\}. \quad (40)$$

Proof: We sum the error-residual formula of equation (33) with $v = \frac{1}{2}(e^k(x_s) - e^{k-2}(x_s))$ from the 2nd to the K time step and substitute in lemmas 1.1, 1.2 and 1.3. This equation is further subsituted into the coercivity property of equation (38) with $w = e^n(x_s)$ and $e^{n-1}(x_s)$ and the symmetric positive definite terms is dropped. Next, we substitute the dual norm of equation (39) with $g(v) = r^n(e^n(x_s); x_s)$ and $r^{n-1}(e^{n-1}(x_s); x_s)$ into the equation, take the norm and apply the inequality $\|b - c\| \leq \|b\| + \|c\|$ followed by another inequality $2|c||d| \leq q|c|^2 + \frac{1}{q}|d|^2$ with $c = \|r^n(x_s)\|_{\mathbf{X}'}$ and $d = \|e^n(x_s)\|$ as well as $c = \|r^{n-1}(x_s)\|_{\mathbf{X}'}$ and $d = \|e^{n-1}(x_s)\|$ together with $q = \frac{2}{\alpha(x_s)}$. Finally, grouping the similar terms together and dropping the $\|e^{n-1}(x_s)\|^2$ term which is always positive proved the lemma [19].

Therefore, the proposition for the *a posteriori* error estimation of the error bound $\Delta_N^k(x_s)$ is developed as the following,

Proposition: for $n = 0, \cdots, K, \|e^n(x_s)\| \leq \Delta_N^n(x_s)$, $\Delta_N^0(x_s) = \Delta_N^1(x_s) = 0,$

$$\Delta_N^2(x_s) \equiv \frac{2}{\alpha(x_s)}\|r^2(x_s)\|_{\mathbf{X}'}, \quad (41)$$

$$\Delta_N^3(x_s) \equiv \frac{2}{\alpha(x_s)}\left(\|r^2(x_s)\|_{\mathbf{X}'} + \|r^3(x_s)\|_{\mathbf{X}'}\right)^{\frac{1}{2}}, \quad (42)$$

and for $n = 4, \cdots, K,$

$$\Delta_N^n(x_s) \equiv \left\{\frac{4}{\alpha(x_s)^2}\left(\|r^n(x_s)\|^2_{\mathbf{X}'} + \|r^{n-1}(x_s)\|^2_{\mathbf{X}'}\right) + \frac{8\Delta t}{\alpha(x_s)}\sum_{j=2}^{n}\left(\left\|\frac{(r^j - r^{j-2})(x_s)}{2\Delta t}\right\|_{\mathbf{X}'}\|e^{j-2}(x_s)\|\right)\right\}^{\frac{1}{2}}. \quad (43)$$

Now, a bound for the reduced basis output error $e_{\mathcal{S}}^k(x_s)$,

Lemma 3: $n = 2, \cdots, K, \quad e_{\mathcal{S}}^0(x_s) = e_{\mathcal{S}}^1(x_s) = 0,$

$$e_{\mathcal{S}}^n(x_s) \leq \|\tilde{\ell}\|_{\mathbf{X}'}\|e^n(x_s)\|. \quad (44)$$

Proof: From the definition of the reduced basis output error $e_{\mathcal{S}}^k(x_s)$, we use the linear property of the output function and the dual norm of equation (39) to prove lemma 3.

Hence, the proposition for the *a posteriori* error estimation of the output error bound $\Delta_{\mathcal{S},N}^k(x_s)$ is,

Proposition: for $n = 0, \cdots, K, e_{\mathcal{S}}^n(x_s) \leq \Delta_{\mathcal{S},N}^n(x_s)$, $\Delta_{\mathcal{S},N}^0(x_s) = \Delta_{\mathcal{S},N}^1(x_s) = 0,$

$$\Delta_{\mathcal{S},N}^n(x_s) \equiv \|\tilde{\ell}\|_{\mathbf{X}'}\Delta_N^n(x_s), \qquad n = 2, \cdots, K. \quad (45)$$

B. Offline-Online Computational Procedures

In order to determine the error bound $\Delta_N^k(x_s)$ and the output error bound $\Delta_{\mathcal{S},N}^k(x_s)$, the dual norm of the residuals $\|r^j(x_s)\|_{\mathbf{X}'}$ and $\|\frac{(r^j - r^{j-2})(x_s)}{2\Delta t}\|_{\mathbf{X}'}$ and output function $\|\tilde{\ell}\|_{\mathbf{X}'}$ must be solved. From standard duality argument, the residual can be expressed as

$$r^k(v; x_s) = (\hat{e}^k(x_s), v), \qquad \hat{e}^k(x_s) \in \mathbf{X}, \quad (46)$$

and substituting into the dual norm of equation (39) and applying the Cauchy-Schwarz inequality, we obtain

$$\|r^k(x_s)\|_{\mathbf{X}'} \leq \frac{\|\hat{e}^k(x_s)\|\|v\|}{\|v\|} = \|\hat{e}^k(x_s)\|. \quad (47)$$

However, if $v = \hat{e}^k(x_s)$, $\|r^k(x_s)\|_{\mathbf{X}'} = \|\hat{e}^k(x_s)\|$ and it is possible for $v = \hat{e}^k(x_s)$ since $\hat{e}^k(x_s) \in \mathbf{X}$,

$$\|r^k(x_s)\|_{\mathbf{X}'} = \|\hat{e}^k(x_s)\|, \quad (48)$$

$$\left\| \frac{(r^k - r^{k-2})(x_s)}{2\Delta t} \right\|_{\mathbf{X}'} = \frac{1}{2\Delta t} \|\hat{e}_r^k(x_s)\|. \quad (49)$$

In a similar fashion, the output function is expressed as

$$\|\tilde{\ell}\|_{\mathbf{X}'} = \|\hat{e}_{\mathcal{S}}\|. \quad (50)$$

Similarly, the *a posteriori* error estimation can be decomposed into offline-online stages [19]. Making use of the affine parametric structure, equation (46) is simplifed into

$$(\hat{e}^k(x_s), v) = \tilde{g}^k \tilde{h}(v) - \sum_{q=1}^{Q_m+Q_a} \sum_{n=1}^{N} \Theta^q(x_s) \lambda_{q,n}^k(x_s) \mathcal{B}^q(\zeta_n, v). \quad (51)$$

When $1 \le q \le Q_m$, $\lambda_{q,n}^k(x_s) = \lambda_{m,n}^k(x_s)$ and $\mathcal{B}^q(\zeta_n, v) = m^q(\zeta_n, v)$. When $Q_m + 1 \le q \le Q_m + Q_a$, $\lambda_{q,n}^k(x_s) = \lambda_{a,n}^k(x_s)$ and $\mathcal{B}^q(\zeta_n, v) = a^q(\zeta_n, v)$. Furthermore

$$\begin{aligned} \tilde{g}^k &= \frac{g^k + g^{k-2}}{2}, \\ \lambda_{m,n}^k(x_s) &= \frac{\underline{P}_{N,n}^k(x_s) - 2\underline{P}_{N,n}^{k-1}(x_s) + \underline{P}_{N,n}^{k-2}(x_s)}{\Delta t^2}, \\ \lambda_{a,n}^k(x_s) &= \frac{\underline{P}_{N,n}^k(x_s) + \underline{P}_{N,n}^{k-2}(x_s)}{2}. \end{aligned}$$

Next, from linear superposition, we write $\hat{e}^k(x_s) \in \mathbf{X}$ as

$$\hat{e}^k(x_s) = \tilde{g}^k \mathcal{C} + \sum_{q=1}^{Q_m+Q_a} \sum_{n=1}^{N} \Theta^q(x_s) \lambda_{q,n}^k(x_s) \mathcal{L}_n^q, \quad (52)$$

for $\mathcal{C} \in \mathbf{X}$ satisfying $(\mathcal{C}, v) = \tilde{h}(v)$, $\forall\, v \in \mathbf{X}$ and $\mathcal{L}_n^q \in \mathbf{X}$ satisfying $(\mathcal{L}_n^q, v) = -\mathcal{B}^q(\zeta_n, v)$, $\forall\, v \in \mathbf{X}$, $1 \le n \le N$, $1 \le q \le Q_m + Q_a$. It thus follows that

$$\|\hat{e}^k(x_s)\|^2 = \Bigg\{ (\tilde{g}^k)^2 (\mathcal{C}, \mathcal{C}) + \sum_{q=1}^{Q_m+Q_a} \sum_{n=1}^{N} \Theta^q(x_s) \lambda_{q,n}^k(x_s) \Bigg\{ 2\tilde{g}^k (\mathcal{C}, \mathcal{L}_n^q) + \sum_{q'=1}^{Q_m+Q_a} \sum_{n'=1}^{N} \Theta^{q'}(x_s) \lambda_{q,n'}^k(x_s) (\mathcal{L}_n^q, \mathcal{L}_{n'}^{q'}) \Bigg\} \Bigg\}. \quad (53)$$

The offline-online computational procedures are now clear. In the offline stage, $\mathcal{C}$ and $\mathcal{L}_n^q$, $1 \le n \le N$, $1 \le q \le Q_m + Q_a$ as well as $\hat{e}_{\mathcal{S}}$, $1 \le n \le N$, are first solved. Next, the system parameters-independent inner products $(\mathcal{C}, \mathcal{C})$, $(\mathcal{C}, \mathcal{L}_n^q)$, $(\mathcal{L}_n^q, \mathcal{L}_{n'}^{q'})$, $1 \le n, n' \le N$, $1 \le q, q' \le Q_m + Q_a$ and $(\hat{e}_{\mathcal{S}}, \hat{e}_{\mathcal{S}})$, $1 \le n \le N$, are evaluated and saved. In the online stage, equation (53) is evaluated by summing the system parameters-dependent terms $\tilde{g}^k$, $\Theta^q(x_s)$ and $\lambda_{q,n}^k(x_s)$ with the stored inner products. Next, the error bound $\Delta_N^k(x_s)$ and the output error bound $\Delta_{\mathcal{S},N}^k(x_s)$ are solved.

The operation counts for the *a posteriori* error estimation in the offline stage is $\mathcal{O}((Q_m + Q_a)^2 N^2 \mathcal{N})$, insignificant compared to the reduced basis operation counts. Similarly, the additional storage counts amount to $\mathcal{O}((Q_m + Q_a) N^2)$, which is equal to the existing reduced basis storage counts. The online stage requires $\mathcal{O}(K(Q_m + Q_a)^2 N^2)$ operation counts, coming from evaluating the last term of equation (53), is slightly more computational expensive than the existing reduced basis operation counts. Hence, the whole reduced basis method and *a posteriori* error estimation requires $\mathcal{O}(\gamma C K \mathcal{N}^\sigma + \gamma K N \mathcal{N})$ operation counts for offline stage, $\mathcal{O}((Q_m + Q_a) N^2)$ storage counts and $\mathcal{O}(K(Q_m + Q_a)^2 N^2)$ operation counts for online stage.

C. Effectivity

We define the maximum error bound

$$\Delta_{N,max} = \max_{x_s \in \Xi_{test}^{x_s}, k \in \Xi_{test}^k} \Delta_N^k(x_s), \quad (54)$$

as the maximum value of the error bound $\Delta_N^k(x_s)$ throughout the test space Ξ_{test}. The effectivity $\eta_N^k(x_s)$ is defined as the ratio of the error bound $\Delta_N^k(x_s)$ over the norm of the reduced basis error $\|e^k(x_s)\|$,

$$\eta_N^k(x_s) = \frac{\Delta_N^k(x_s)}{\|e^k(x_s)\|}, \quad (55)$$

while the maximum effectivity

$$\eta_{N,max} = \max_{x_s \in \Xi_{test}^{x_s}, k \in \Xi_{test}^k} \eta_N^k(x_s), \quad (56)$$

is the maximum value of the effectivity $\eta_N^k(x_s)$ throughout the test space Ξ_{test}.

Furthermore, the maximum bound-maximum error ratio

$$\xi_{N,max} = \frac{\Delta_{N,max}}{\|e\|_{te,max}}, \quad (57)$$

is defined as the ratio of the maximum error bound $\Delta_{N,max}$ over the maximum norm of the reduced basis error $\|e\|_{te,max}$ in the test space Ξ_{test}.

The maximum effectivity $\eta_{N,max}$ remain constant at a magnitude of $\mathcal{O}(10^3)$. However, at later stage, the maximum effectivity $\eta_{N,max}$ increases rapidly. It is observed that at somewhere in the test space Ξ_{test}, "peaks" of exceptionally high effectivity $\eta_N^k(x_s)$ is present. These "peaks" correspond to a time step where the norm of the reduced basis error

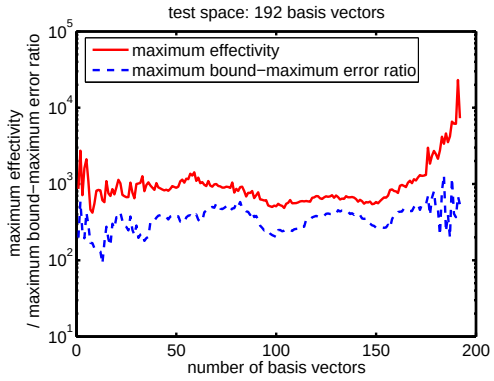

Fig. 6. Convergence rate of the maximum effectivity $\eta_{N,max}$ and maximum bound-maximum error ratio $\xi_{N,max}$ (right) in test space Ξ_{test}.

$\|e^k(x_s)\|$ is exceptionally low due to the greedy algorithm selecting a basis vector near that region. However, this is not a concern because this means that the reduced basis pressure distribution $P_N^k(x_s)$ is closer to the finite element pressure distribution $P^k(x_s)$.

From figure (6), it can be seen that the maximum bound-maximum error ratio $\xi_{N,max}$ has roughly a constant value of 400, which correspond to the 2 orders of magnitude difference between the maximum error bound $\Delta_{N,max}$ and the maximum norm of the reduced basis error $\|e\|_{te,max}$. This implies that the effectivity $\eta_N^k(x_s)$ does not blow up when the norm of the reduced basis error $\|e^k(x_s)\|$ is large.

VI. Inverse Problem

A. Formulation

As the occurring time T has a role to play in the inverse problem, the system parameters $\mu \equiv \{x_s, T\}$ is used. We assume that, for the one-dimensional seismic problem, the actual system parameters $\mu^* \in \mathcal{D}$ (though fixed) is unknown and must be determined in real-time by appropriate comparison of field measurements and the reduced basis output $\mathcal{S}_N^k(\mu)$. We assume that the output $\mathcal{S}^k(\mu)$ is recorded at a total of $\mathcal{K}$ different time steps and conclude from these field data,

$$\mathcal{S}^{k_i}(\mu) \in \mathcal{E}^{k_i}, \qquad 1 \le i \le \mathcal{K}. \tag{58}$$

$\mathcal{S}^{k_i}(\mu)$ denotes the output $\mathcal{S}^k(\mu)$ at the particular k_i time step and $\mathcal{E}^{k_i} \equiv [\mathcal{E}_-^{k_i}, \mathcal{E}_+^{k_i}]$ denotes the measured field error where $\mathcal{E}_-^{k_i}$ and $\mathcal{E}_+^{k_i}$ are the lower and upper measured field error respectively. We thus provide a "possibility region" $\mathcal{P}$ which corresponds to all possible system parameters μ consistent with the field data. Each k_i time step will provide its own "individual possibility region" $\mathcal{P}_i$ and their intersection will give the "possibility region" $\mathcal{P}$. Hence, it is easy to deduce that the "possibility region" $\mathcal{P}$ can be expressed as

$$\mathcal{P} = \bigcap_{1 \le i \le \mathcal{K}} \mathcal{P}_i, \tag{59}$$

$$\mathcal{P}_i = \{\mu \in \mathcal{D} \mid \mathcal{S}^{k_i}(\mu) \in \mathcal{E}^{k_i}\}, \quad 1 \le i \le \mathcal{K}. \tag{60}$$

The output bound gap $\mathcal{S}_\Delta^k(\mu) \equiv [\mathcal{S}_{\Delta,-}^k(\mu), \mathcal{S}_{\Delta,+}^k(\mu)]$ consists of the lower output bound

$$\mathcal{S}_{\Delta,-}^k(\mu) = \mathcal{S}^k(\mu) - \Delta_{\mathcal{S},N}^k(\mu), \tag{61}$$

and the upper output bound

$$\mathcal{S}_{\Delta,+}^k(\mu) = \mathcal{S}^k(\mu) + \Delta_{\mathcal{S},N}^k(\mu). \tag{62}$$

Lastly, we define an inverse space $\Xi_{inverse} = \Xi_{inverse}^{x_s} \times \Xi_{inverse}^{T}$: a system parameters space containing τ different system parameters μ.

The procedure is as follow:

Step 1. Perform the online stage in the inverse space $\Xi_{inverse}$.

Step 2. Obtain the reduced basis output $\mathcal{S}_N^{k_i}(\mu)$ as well as its output error bound $\Delta_{\mathcal{S},N}^{k_i}(\mu)$ for all k_i time steps, $1 \le i \le \mathcal{K}$ and calculate the output bound gap $\mathcal{S}_\Delta^{k_i}(\mu)$.

Step 3. Compare the output bound gap $\mathcal{S}_\Delta^{k_i}(\mu)$ with the measured field error $\mathcal{E}^{k_i}$; if the output bound gap $\mathcal{S}_\Delta^{k_i}(\mu)$ is outside the measured field error $\mathcal{E}^{k_i}$,

$$\mathcal{S}_{\Delta,-}^{k_i}(\mu) > \mathcal{E}_+^{k_i}, \quad \text{or} \quad \mathcal{S}_{\Delta,+}^{k_i}(\mu) < \mathcal{E}_-^{k_i}, \tag{63}$$

that corresponding system parameters μ is not the actual system parameters μ^*. Taking the complement will give us the "individual possibility region" $\mathcal{P}_i$ for the k_i time step.

Step 4. The intersection of the $\mathcal{K}$ different "individual possibility region" $\mathcal{P}_i$ from the various k_i time steps will give the "possibility region" $\mathcal{P}$.

As our "possibility region" are based on rigorous output bounds, the fast approximation of the actual system parameters is guaranteed to be conservative and accurate.

B. Results

By considering an "unknown" (to the code but known to us) actual system parameters μ^*, we observed that the time step used affects the "individual possibility region" $\mathcal{P}_i$. When the particular k_i time step selected correspond to the distinct characteristic of the reduced basis output $\mathcal{S}_N^k(\mu)$, the "individual possibility region" $\mathcal{P}_i$ is small, as seen in figure (7). Hence, we fixed the total number of time steps used for comparison as $\mathcal{K} = 9$, equally spaced to ensure sampling of at least 1 time step in the distinct characteristic region. Lastly, the measured field error $\mathcal{E}^{k_i}$ is created from the reduced basis output $\mathcal{S}_N^k(\mu)$ by specifying an arbitrary $\mathcal{E}_f\%$ field error range, $\mathcal{E}_\pm^{k_i} = \mathcal{S}_N^{k_i}(\mu) \pm \frac{\mathcal{E}_f\%}{2}$.

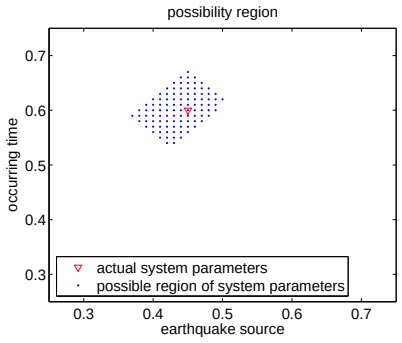

Fig. 7. "Possibility region" $\mathcal{P}$ when total number of time steps used for comparison are $\mathcal{K} = 9$.

VII. Conclusion

We developed the reduced basis method, offline-online computational procedures and corresponding *a posteriori* error estimation for the one-dimensional seismic problem, governed by the second order wave equation which is hyperbolic, linear in nature, with smooth initial pressure and rate of pressure change with time. Next, we performed the inverse problem.

We have shown that the reduced basis pressure distribution $P_N^k(x_s)$ is an accurate approximation to the finite element pressure distribution $P^k(x_s)$ and the accuracy increases as the dimension of the reduced basis space N increases. The offline-online computational procedures work well although the convergence rate is slow. This may be due to the nature of the finite element pressure solution $P^k(x_s)$, which is not smooth enough across the earthquake source-time space.

As the dimension of the finite element space $\mathcal{N}$ is comparable with the dimension of the reduced basis space N for the one-dimensional seismic problem, the saving in computational cost when applying the online stage instead of the finite element method is not experienced. We should expect the saving in computational cost to be experienced in the two-dimensional seismic problem.

We developed the *a posteriori* error estimation for the error bound $\Delta_N^k(x_s)$ and output error bound $\Delta_{S,N}^k(x_s)$. Results show that the maximum effectivity $\eta_{N,max}$ has a magnitude of $\mathcal{O}(10^3)$ which increases rapidly when the tolerance ε is lower. However, this is due to a low value for the norm of the reduced basis error $\|e^k(x_s)\|$. The maximum bound-maximum error ratio $\xi_{N,max}$ gives a constant magnitude of $\mathcal{O}(10^2)$, showing that effectivity $\eta_N^k(x_s)$ does not blow up during a high value for the norm of the reduced basis error $\|e^k(x_s)\|$.

Finally, the inverse problem works well, giving a "possibility region" $\mathcal{P}$ of system parameters μ where the actual system parameters μ^* may be in. We further observed that the k_i time steps selected for comparison should correspond to the distinct characteristic of the reduced basis output $\mathcal{S}_N^k(\mu)$ in order to have a small "possibility region" $\mathcal{P}$.

References

[1] B. O. Almroth, P. Stern, and F. A. Brogan. Automatic choice of global shape functions in structural analysis. *AIAA Journal*, 16:525–528, May 1978.

[2] A. K. Noor and J. M. Peters. Reduced basis technique for nonlinear analysis of structures. *AIAA Journal*, 18(4):455–462, April 1980.

[3] E. Balmes. Parametric families of reduced finite element models: Theory and applications. *Mechanical Systems and Signal Processing*, 10(4):381–394, 1996.

[4] J. P. Fink and W. C. Rheinboldt. On the error behavior of the reduced basis technique for nonlinear finite element approximations. *Z. Angew. Math. Mech.*, 63:21–28, 1983.

[5] T. A. Porsching. Estimation of the error in the reduced basis method solution of nonlinear equations. *Mathematics of Computation*, 45(172):487–496, October 1985.

[6] W. C. Rheinboldt. On the theory and error estimation of the reduced basis method for multi-parameter problems. *Nonlinear Analysis, Theory, Methods and Applications*, 21(11):849–858, 1993.

[7] M. D. Gunzburger. *Finite Element Methods for Viscous Incompressible Flows: A Guide to Theory, Practice, and Algorithms*. Academic Press, Boston, 1989.

[8] K. Ito and S. S. Ravindran. A reduced-order method for simulation and control of fluid flows. *Journal of Computational Physics*, 143(2):403–425, July 1998.

[9] J. S. Peterson. The reduced basis method for incompressible viscous flow calculations. *SIAM J. Sci. Stat. Comput.*, 10(4):777–786, July 1989.

[10] C. Prud'homme, D. Rovas, K. Veroy, Y. Maday, A.T. Patera, and G. Turinici. Reliable real-time solution of parametrized partial differential equations: Reduced-basis output bounds methods. *Journal of Fluids Engineering*, 124(1):70–80, Mar 2002.

[11] Y. Maday, A.T. Patera, and G. Turinici. Global a priori convergence theory for reduced-basis approximation of single parameter symmetric coercive elliptic partial differential equations. *C. R. Acad. Sci. Paris, Série I*, 335(3):289–294, 2002.

[12] Martin A. Grepl. *Reduced-Basis Approximation and A Posteriori Error Estimation for Parabolic Partial Differential Equations*. PhD thesis, Massachusetts Institute of Technology, 2005.

[13] K. Veroy. *Reduced Basis Methods Applied to Problems in Elasticity: Analysis and Applications*. PhD thesis, Massachusetts Institute of Technology, 2003.

[14] Karen Veroy, Christophe Prudhomme, and Anthony T. Patera. Reduced-basis approximation of the viscous burgers equation: Rigorous a posteriori error bounds. *C. R. Acad. Sci. Paris, Série I*, 337(9):619–624, 2003.

[15] Hesheng Bao, Jacobo Bielak, Omar Ghattas, Loukas F. Kallivokas, David R. O'Hallaron, Jonathan R. Shewchuk, and Jifeng Xu. Large-scale simulation of elastic wave propagation in heterogeneous media on parallel computers. *Computer Methods in Applied Mechanics and Engineering*, 152(1–2):85–102, January 1998.

[16] Hesheng Bao, Jacobo Bielak, Omar Ghattas, David R. O'Hallaron, Loukas F. Kallivokas, Jonathan Richard Shewchuk, and Jifeng Xu. Earthquake ground motion modeling on parallel computers. In *Supercomputing '96*, Pittsburgh, Pennsylvania, November 1996.

[17] Jacobo Bielak, Yoshiaki Hisada, Hesheng Bao, Jifeng Xu, and Omar Ghattas. One- vs two- or three-dimensional effects in sedimentary valleys. In *Proceedings of 12th World Conference on Earthquake Engineering*, Aukland, New Zealand, 2000.

[18] Volkan Akcelik, Jacobo Bielak, George Biros, Ioannis Epanomeritakis, Antonio Fernandez, Omar Ghattas, Eui Joong Kim, Julio Lopez, David O'Hallaron, Tiankai Tu, and John Urbanic. High resolution forward and inverse earthquake modeling on terasacale computers. In *Proceedings of SC2003*, Phoenix, AZ, November 2003.

[19] Alex Y.K. Tan. Reduced basis method for 2nd order wave equation: Application to one-dimensional seismic problem. Master's thesis, Massachusetts Institute of Technology, 2006.

[20] N. C. Nguyen, K. Veroy, and A. T. Patera. Certified real-time solution of parametrized partial differential equations. In S. Yip, editor, *Handbook of Materials Modeling*, pages 1523–1558. Springer, 2005.